Electronic supplementary information

Promoting Oxygen Reduction *via* Coordination Environment Modulation through Secondary Metal-atom Incorporation

*Haozhou Yang[a], Tianyu Zhang[a], Xiao Chi[b], Xiaojiang Yu[b], Junmei Chen[a], Jiayi Chen[a], Chunfeng Li[a], Shengdong Tan[c], Qian He[c], Xun Wang[d] and Lei Wang[a]**

[a] *Department of Chemical and Biomolecular Engineering, National University of Singapore, 117585 Singapore*

[b] *Department of Physics and Singapore Synchrotron Light Source, National University of Singapore, 119077 Singapore*

[c] *Department of Material Science Engineering, National University of Singapore, 117575 Singapore*

[d] *Key Lab of Organic Optoelectronics and Molecular Engineering, Department of Chemistry, Tsinghua University, Beijing 100084, China*

E-mail: wanglei8@nus.edu.sg

Experimental procedures

Chemicals: $Zn(NO_3)_2$, $Cu(NO_3)_2$, $Fe(NO_3)_3$, 2-methylimidazole (2-Hmim), polyvinylpyrrolidone (PVP) K30, N,N-dimethylformamide (DMF), KOH and H_2SO_4 were purchased from Sigma-Aldrich in analytical grade, methanol was obtained from Fisher Chemical. All the reagents were used as received without further purification.

Synthesis of ZnCu-ZIF: In a typical synthesis, 80 mg $Zn(NO_3)_2$, 20 mg $Cu(NO_3)_2$, 120 mg 2-Hmim and 110 mg PVP were dissolved in a mixture of 9.6 mL DMF and 16 mL methanol. After 10 minutes magnetic stirring, the solution was transferred into a 50-mL Teflon-lined stainless-steel autoclave. The sealed vessel was then heated at 120℃ for 12 h before it was cooled down to room temperature. The products were separated via centrifugation at 9000 rpm for 4 min and further washed with methanol for several times.

Synthesis of ZnCuFe$_x$-ZIF: Similar with synthesis of ZuCu-ZIF but with addition of x mg $Fe(NO_3)_3$ (x = 5, 10, 20 mg).

Synthesis of ZnFe10-ZIF: Similar with synthesis of ZuCu-ZIF but with replacement of 20 mg $Cu(NO_3)_2$ to 10 mg $Fe(NO_3)_3$.

Synthesis of Cu-900: In a typical synthesis, 25 mg as-prepared ZuCu-ZIF was put in porcelain boat and calcinated at 900 ℃ for 4 h with a heating rate of 5 ℃ min^{-1} under flowing Ar atmosphere and cooled down to room temperature before collected.

Synthesis of CuFex-900: In a typical synthesis, 25 mg as-prepared ZnCuFe$_x$-ZIF was put in porcelain boat and calcinated at 900 ℃ for 4 h with a heating rate of 5 ℃ min^{-1} under flowing Ar atmosphere and cooled down to room temperature before collected.

Synthesis of Fe10-900: In a typical synthesis, 15 mg as-prepared ZnFe-ZIF was put in porcelain boat and calcinated at 900 ℃ for 4 h with a heating rate of 5 ℃ min^{-1} under flowing Ar atmosphere and cooled down to room temperature before collected.

Synthesis of CuFe10-800 and CuFe10-1000: Similar with synthesis of Fe10-900 but with calcination temperature of 800 ℃ or 1000 ℃ instead.

Materials characterization: Powder X-ray diffraction (PXRD) patterns were recorded on a Bruker D8-advance X-ray powder diffractometer operated at 40 kV voltage and 30 mA current with CuKα radiation (λ=1.5406 Å). High-resolution transmission electronic microscope (HRTEM) and high-angle annular dark-field scanning TEM (HAADF-STEM), energy dispersive spectroscopy (EDS) elemental mapping spectra were obtained by a JEOL JEM-2100F operating at 200 kV. HAADF-STEM image shown in Figure 1e was taken using an aberration-corrected JEOL JEM200CF operating at 200kV at the National University of Singapore. The scanning electron microscope (SEM) was carried out on a JEOL JEM-7610M equipped with energy dispersive X-ray spectrometer (EDS) analyzed at 15 kV. X-ray photoelectron spectroscopy (XPS) was performed on scanning X-ray microprobe (Kratos Axis Ultra DLD) operated at 15 kV, 1486.71 eV with monochromated Al Kα radiation. Binding energies were corrected by reference to the C 1s peak at 284.8 eV. Gas sorption isotherms were obtained with Micromeritics TriStar II3020 and Micromeritics ASAP 2020 M+C accelerated surface area and porosimetry analyzers at a set temperature. The samples were degassed at 120 ℃ for 6 h. The obtained adsorption-desorption isotherms were evaluated to give the pore parameters, including Brunauer-Emmett-Teller (BET) specific surface area, and pore size. The pore size distribution was calculated with BJH method using the desorption branch. Element weight proportion was measured by inductively coupled plasma optical emission spectrometer (ICP-OES, ThermoFisher CCAPG200 DUO). X-ray absorption fine spectroscopy (XAFS) data were recorded at beamline 1W1B station in Beijing Synchrotron Radiation Facility (BSRF). Soft X-ray absorption spectroscopy measurements were performed at the SINS beamline of Singapore Synchrotron Light Source (SSLS). The energy resolution was set ~0.1eV. The C K-edge absorption data are collected in total electron yield (TEY) mode monitoring total current.

The base pressure in the UHV chamber is maintained at ~2 × 10^{-10} mbar throughout the measurements.

Electrochemical measurements: The electrochemical performance was evaluated using a three-electrode system on BioLogic VMP3e electrochemical workstation. An Ag/AgCl electrode and a graphite rod electrode serve as reference electrode and counter electrode, respectively. A rotating risk disk electrode set-up (RRDE, Pine Inc.) serves as working electrode. The catalyst suspension ink was prepared by dispersing 1 mg of catalyst and 7 μL of 5% Nafion (Sigma-Aldrich) in 53 μL 3:1 isopropanol-water mixture and sonicated for at least 30 min. The as-prepared ink was pipetted onto glassy carbon ring disk by 7 μL, then dried in fume hood. The loading of active materials was around 0.47 mg cm^{-2}. Commercial 20% Pt/C (E-TEK) was selected as reference materials with loading amount of around 0.8 mg cm^{-2}. All potentials were converted to a reversible hydrogen electrode via a RHE calibration according to previous literature and shown in Fig. S14.[1]

The measurements were performed in O_2 saturated 0.1 M KOH aqueous solution. Polarization curves were carried out at the scan rate of 5 mV s^{-1} with rotating rate of 1600 rpm. Tafel plot was acquired with LSV method from 0.95 V to 0.8 V at the scan rate of 2 mV s^{-1}. Stability test was conducted with chronoamperometric method at the fixed potential of 0.85 V vs. RHE using carbon fiber paper (Toray H060) as working electrode. The electron-transfer number (n) was evaluated with Koutecky–Levich (K-L) equation:[2]

$$\frac{1}{J}=\frac{1}{J_L}+\frac{1}{J_K}=\frac{1}{B\omega^{0.5}}+\frac{1}{J_K}$$

$$B = 0.62nFC_0\,(D_0)^{2/3}\,\nu^{-1/6}$$

J is the measured current density,

J_K and J_L are the kinetic and diffusion-limiting current densities,

ω is the angular velocity ($\omega=2\pi N$, N is rotating rate),

n is electron transfer number,

F is the Faraday constant (96485 C mol^{-1}),

C_0 is the bulk concentration of O_2 (1.2×10^{-6} mol cm^{-3} for 0.1 M KOH),

D_0 is the diffusion coefficient of O_2 (1.9×10^{-5} cm^2 s^{-1} in 0.1 M KOH),

and v is the kinematic viscosity of the electrolyte (0.01 cm^2 s^{-1} in 0.1 M KOH).

J_k was calculated according to equation:

$$\frac{1}{J_K}=\frac{1}{J}-\frac{1}{J_L}=\frac{1}{J}-\frac{1}{1.4573\times n}$$

J is current density at definite potential (0.9 V vs. RHE here), and n is electron transfer number.

The hydrogen peroxide yield (H_2O_2 %) and the electron transfer number (n) were also calculated by the followed equations:

$$n=\frac{4\times i_d}{\frac{i_d}{N}+i_r}$$

$$H_2O_2\ (\%)=\frac{200\times i_r}{N\times i_d+i_r}$$

Where i_r and i_d are the measured ring and disk currents respectively. N is collecting efficiency (0.38) of RRDE. The ring potential was set to 1.48 V vs. RHE.

Electrochemical surface area (ECSA) of catalysts was evaluated by the equation:

ECSA= C_{dl}/C_s

while C_{dl} is the electrochemical double-layer capacitance derived from the slope of linear fit of the current density against scan rate (10, 15, 20, 25, 30 mV/s), which were determined in Fig. S24 by the cyclic voltammograms (CVs) at non-faradic potential window between 1.07 ~ 1.21 V vs. RHE. The C_s is the specific capacitance assumed to be 20 μF cm^{-2} for a smooth planar

surface. Therefore, the ECSA of Cu-900, Fe10-900 and CuFe10-900 are 555, 550 and 595 cm^2_{ECSA} respectively.

Fabrication of Zn-air battery: The Zn-air battery was fabricated using a home-made cell. The catalyst was loaded on the gas diffusion layer with microporous carbon layer (1.5 ×1.5 cm^2, Sigracet 29BC, FuelCellStore) as air electrode. copper foil was employed as current collector. The loading amount is around 1 mg cm^{-2}. A polished zinc foil was used as the anode. The area of the electrodes exposed to the electrolyte is 1cm^2. The electrolyte was a mixture of 6.0 M KOH and 0.2 M $ZnAc_2$. All characterizations were recorded on BioLogic VMP3e electrochemical workstation.

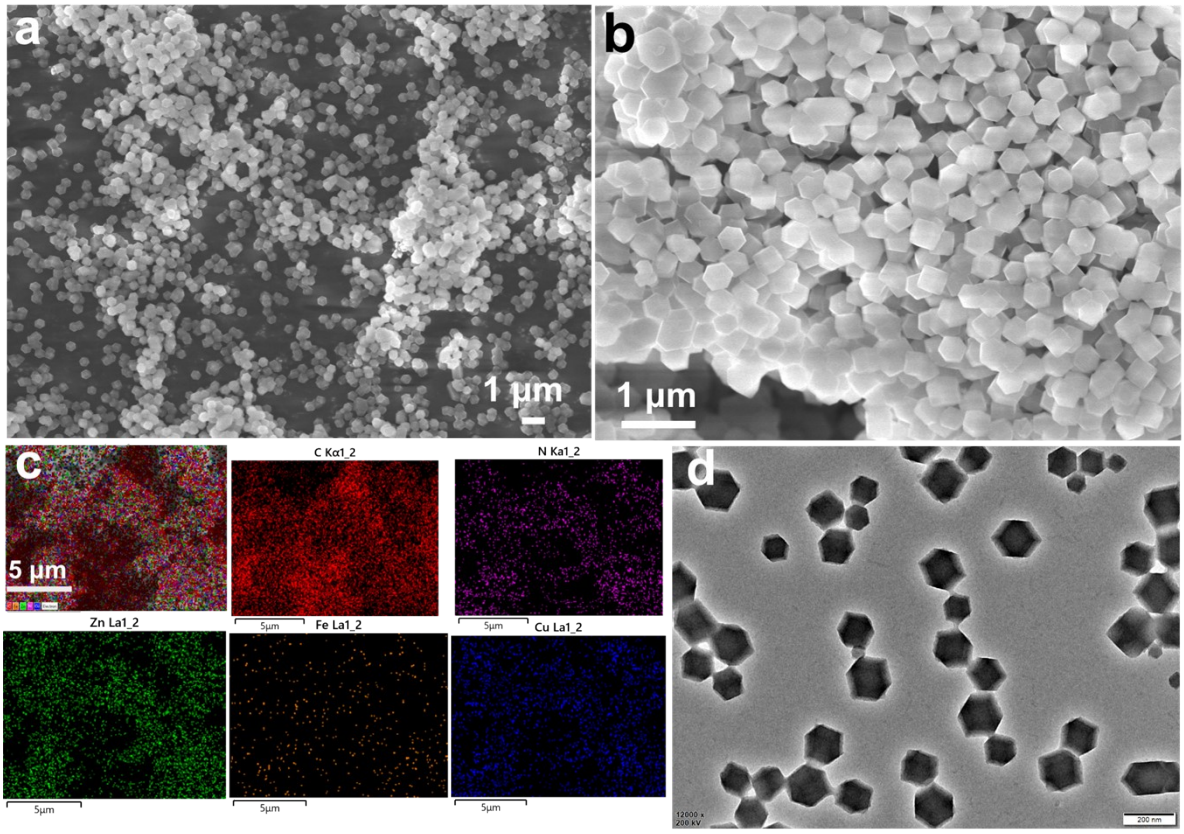

Fig. S1. a-b) FESEM image with different magnification scales, c) EDS elemental mapping images, d) TEM images of ZnCuFe10-ZIF.

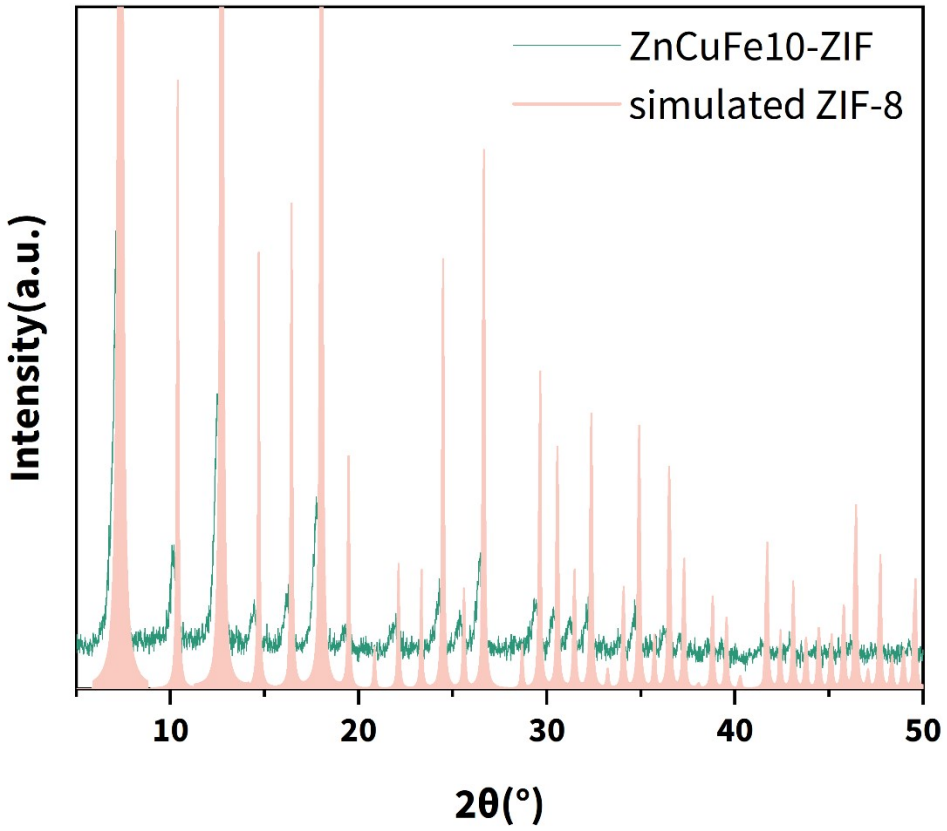

Fig. S2. XRD pattern of ZnCuFe10-ZIF.

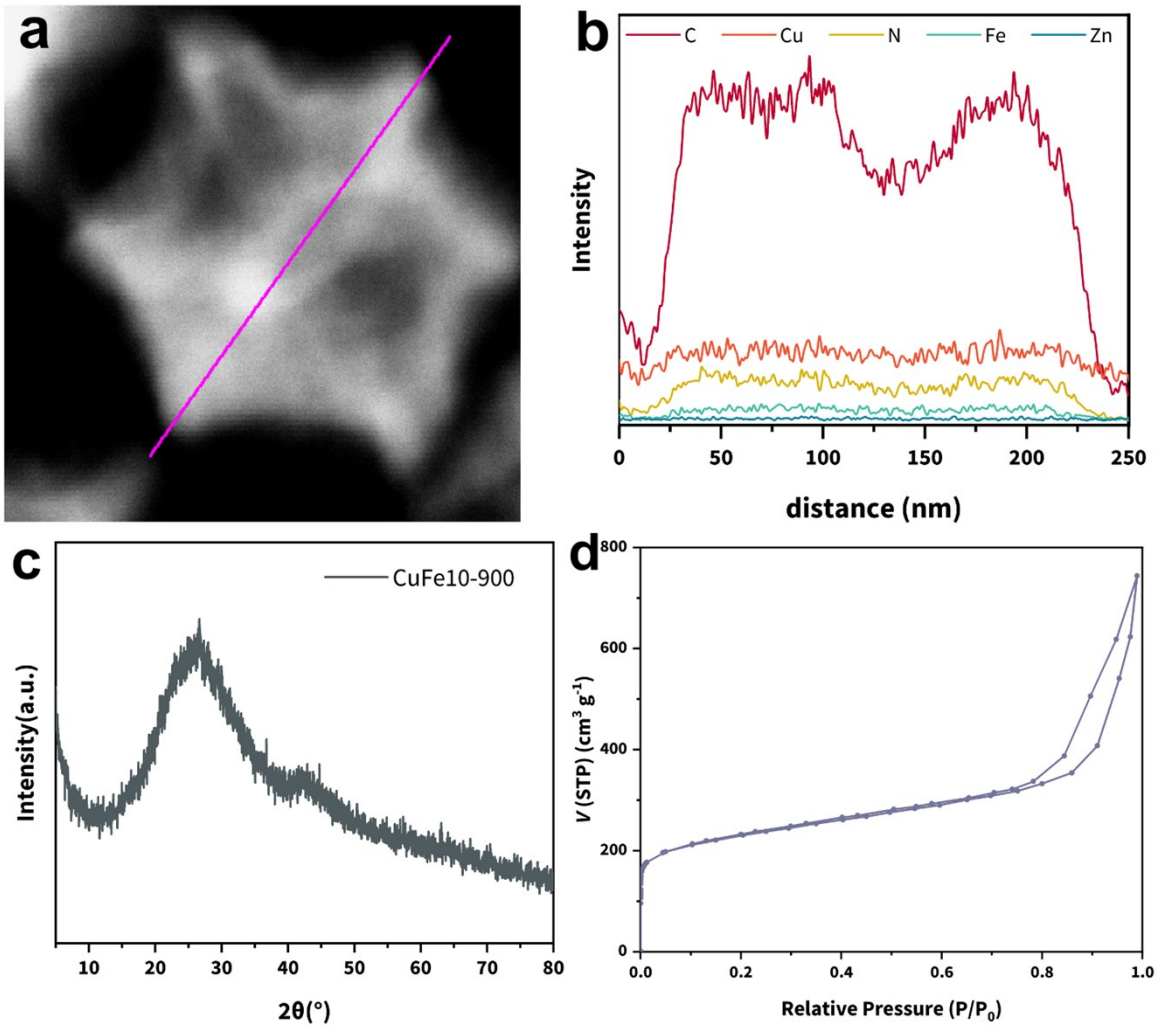

Fig. S3. a) HAADF-STEM image and b) corresponding EDS elemental line scanning profile, c) XRD pattern and d) N_2 adsorption-desorption isotherm of CuFe10-900.

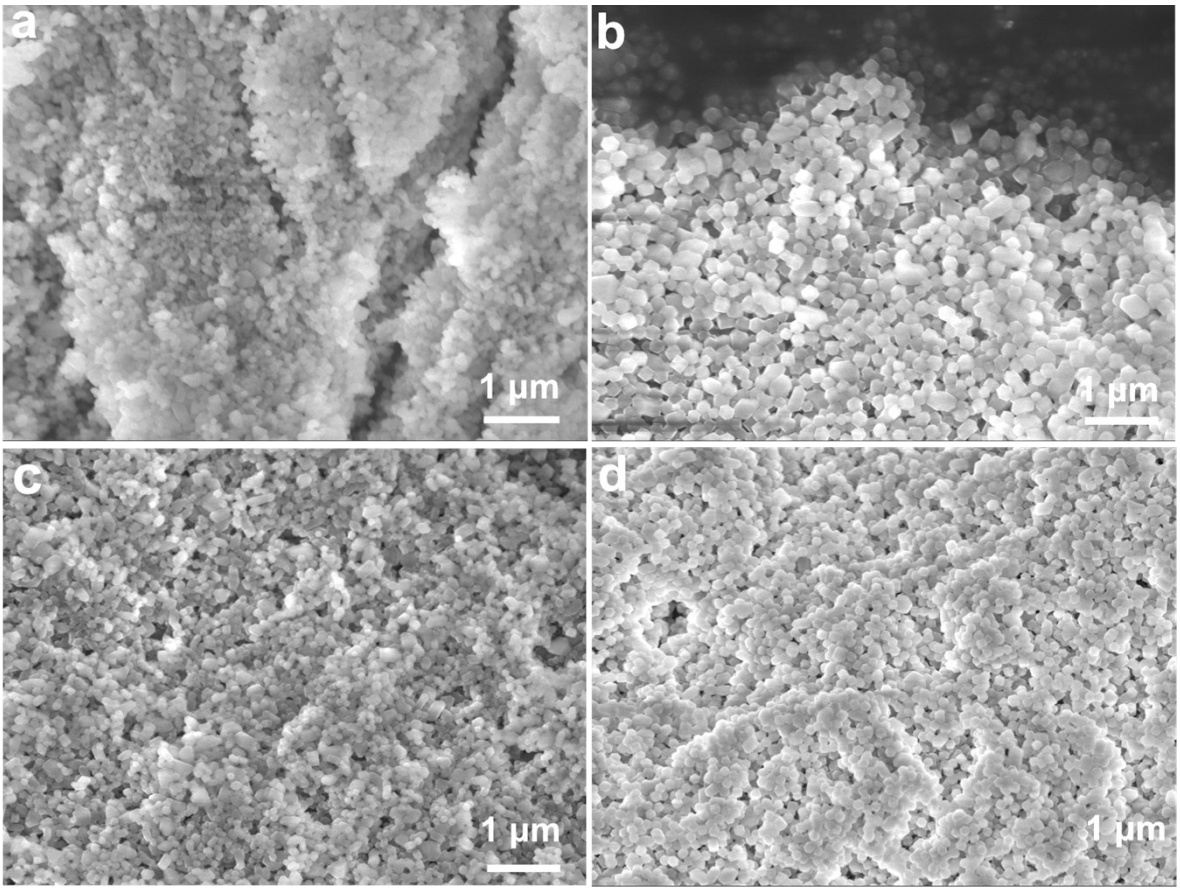

Fig. S4. SEM images of different ZIF analogues. a) ZnCu-ZIF, b) ZnFe10-ZIF, c) ZnCuFe5-ZIF and d) ZnCuFe20-ZIF.

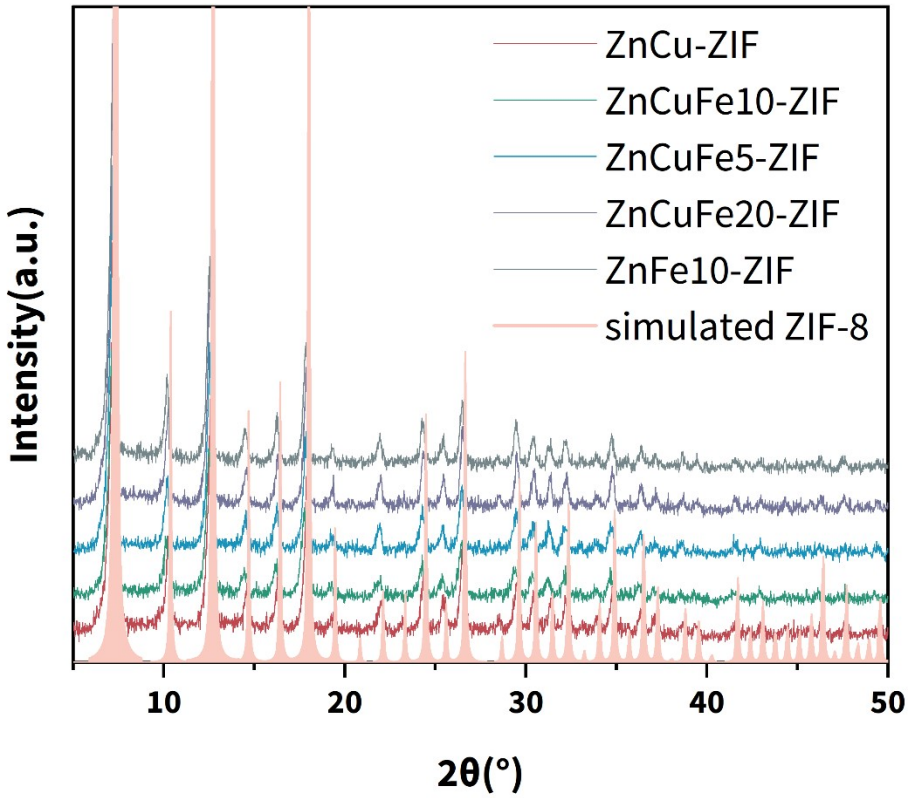

Fig. S5. XRD patterns of different ZIF precursors as well as simulated ZIF-8 pattern.

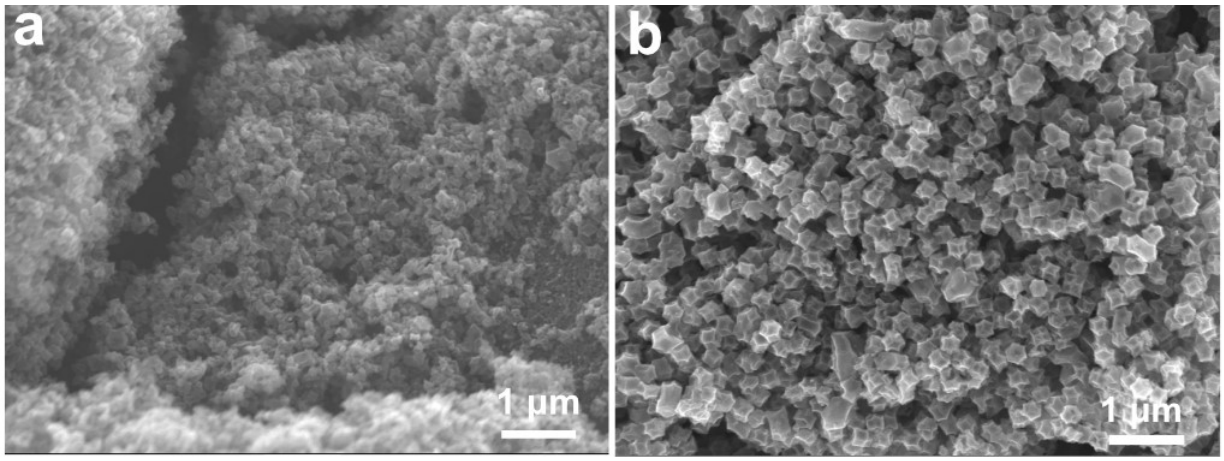

Fig. S6. SEM images of different SACs. a) Cu-900, b) Fe10-900.

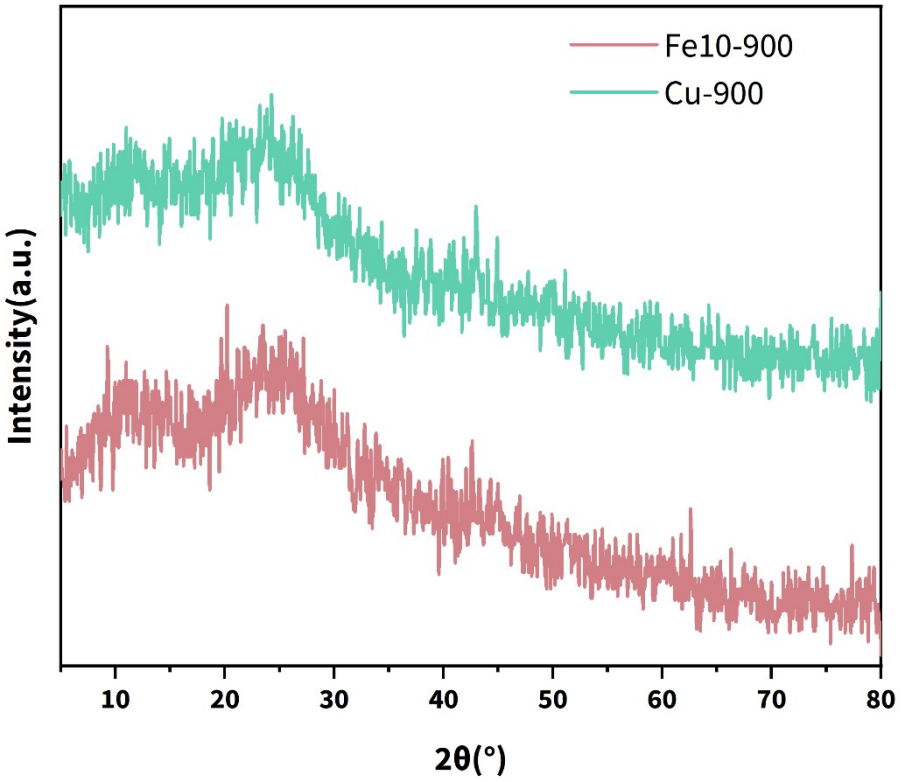

Fig. S7. XRD patterns of Cu-900 and Fe10-900.

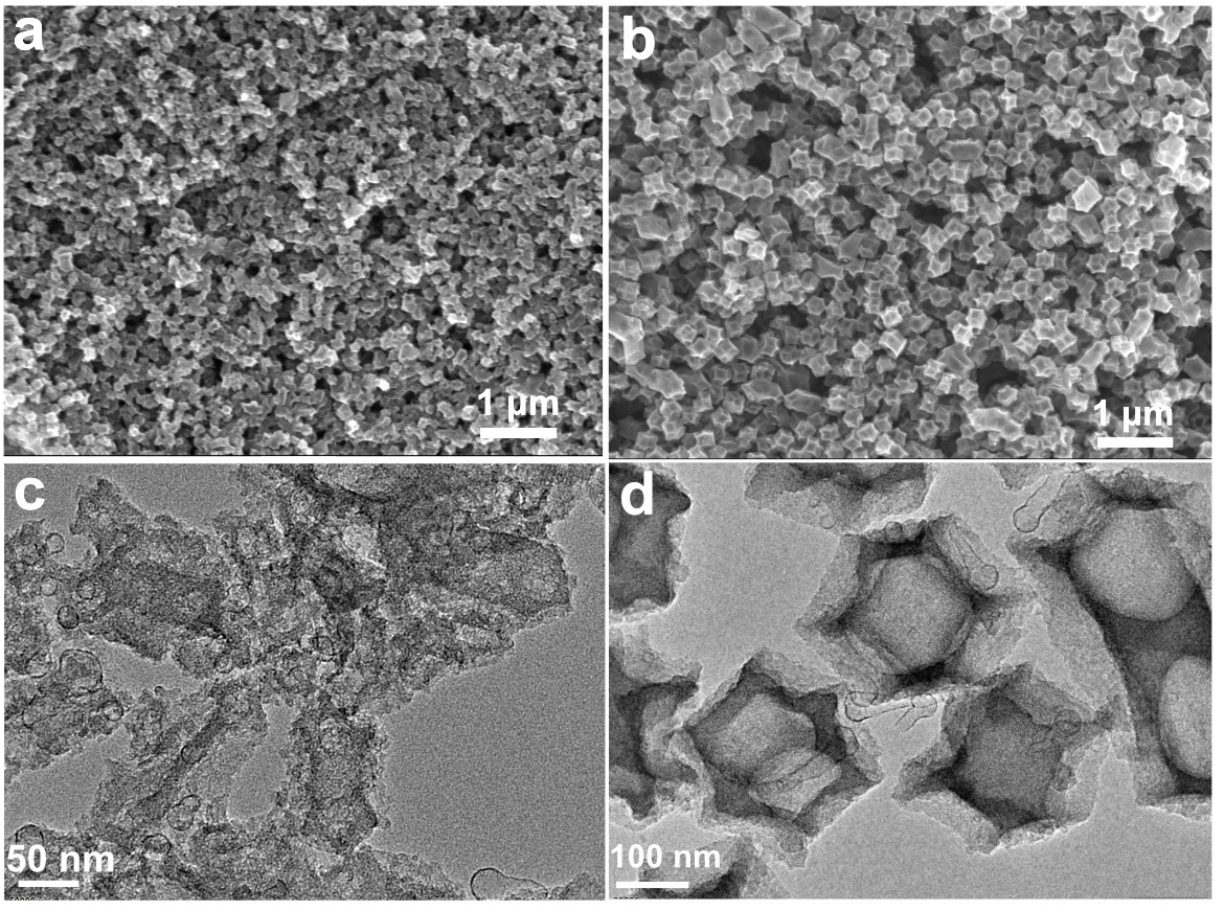

Fig. S8. SEM images a) CuFe5-900, b) CuFe20-900; TEM images of c) CuFe5-900, d) CuFe20-900.

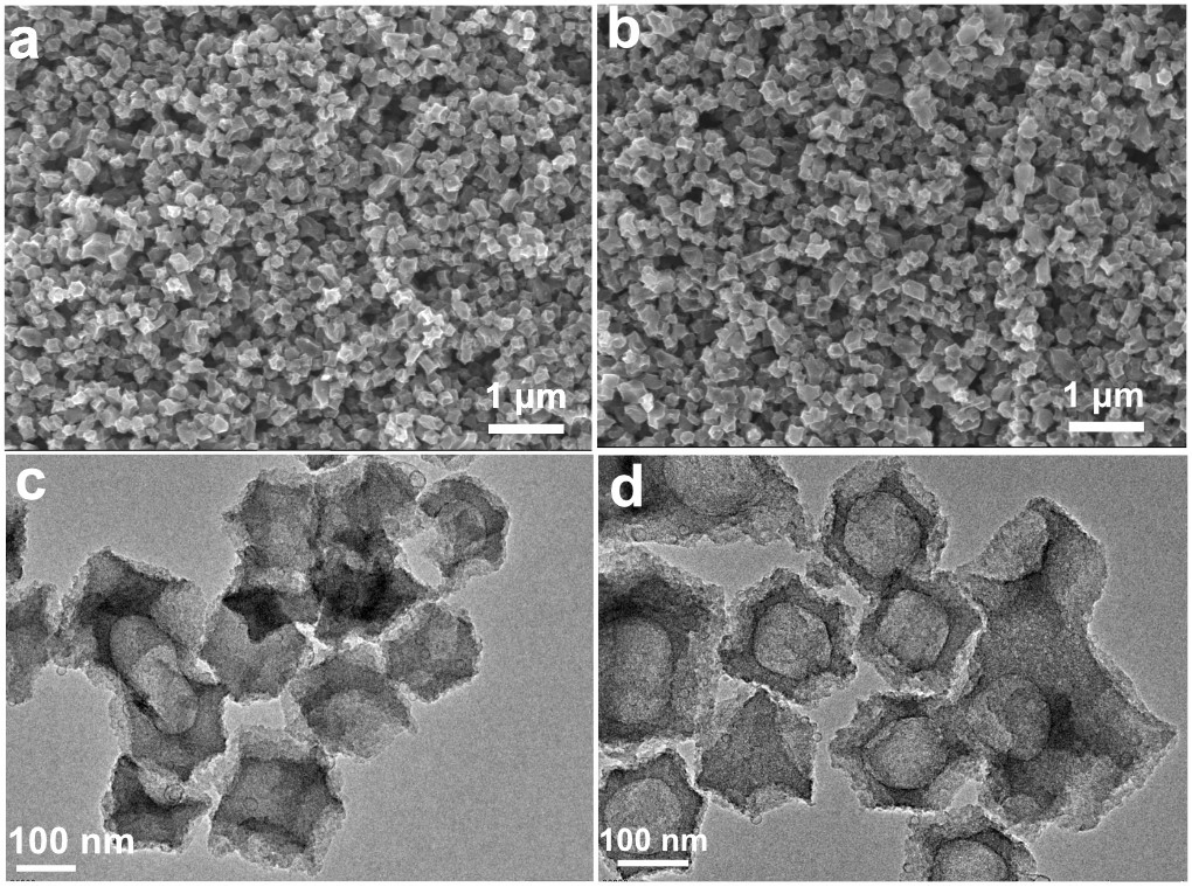

Fig. S9. SEM images of a) CuFe10-800 and b) CuFe10-1000; TEM images of c) CuFe10-800 and d) CuFe10-1000.

samples	Zn (%)	Cu (%)	Fe (%)
ZnCuFe10-ZIF	23.33%	1.45%	1.07%
ZnCuFe5-ZIF	19.89%	1.18%	0.60%
ZnCuFe20-ZIF	24.08%	1.37%	2.88%
CuFe10-900	0.01%	2.40%	2.42%
Cu-900	0.22%	3.68%	-
Fe10-900	0.01%	-	2.93%
CuFe5-900	0.09%	4.71%	1.54%
CuFe20-900	0.12%	3.19%	4.57%
CuFe10-800	5.19%	2.15%	1.29%
CuFe10-1000	0.01%	3.15%	3.51%

Table S1. Elemental proportions in different ZIF precursors and SACs determined by ICP-OES.

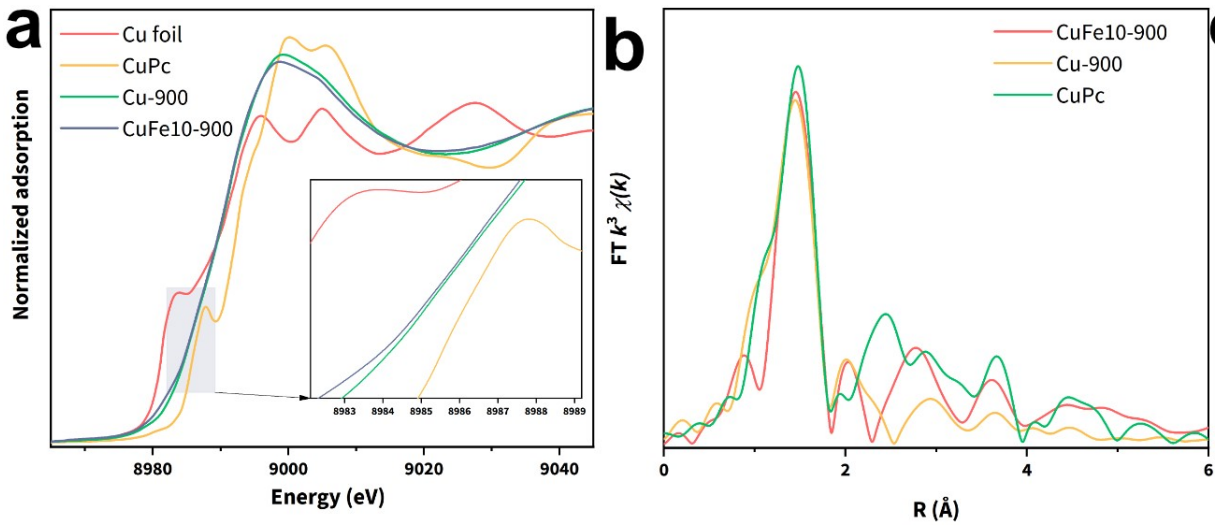

Fig. S10. XANES and FT-EXAFS spectra of Cu K-edge for different samples.

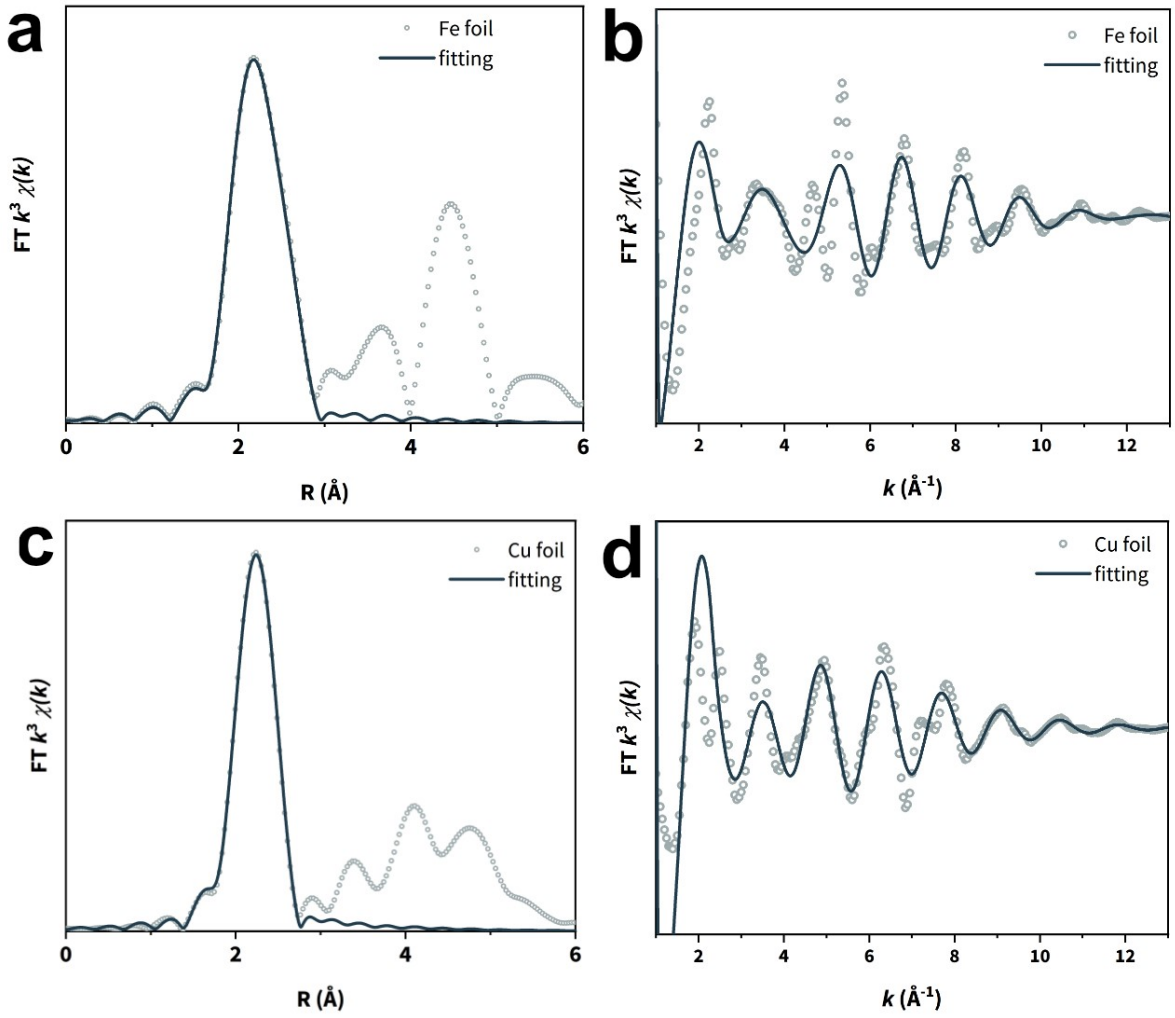

Fig. S11. first-shell Fe-Fe single scattering path fitting of a) *R* space and b) *k* space of Fe K-edge EXAFS spectra of Fe foil; first-shell Cu-Cu single scattering path fitting of c) *R* space and d) *k* space of Cu K-edge EXAFS spectra of Cu foil.

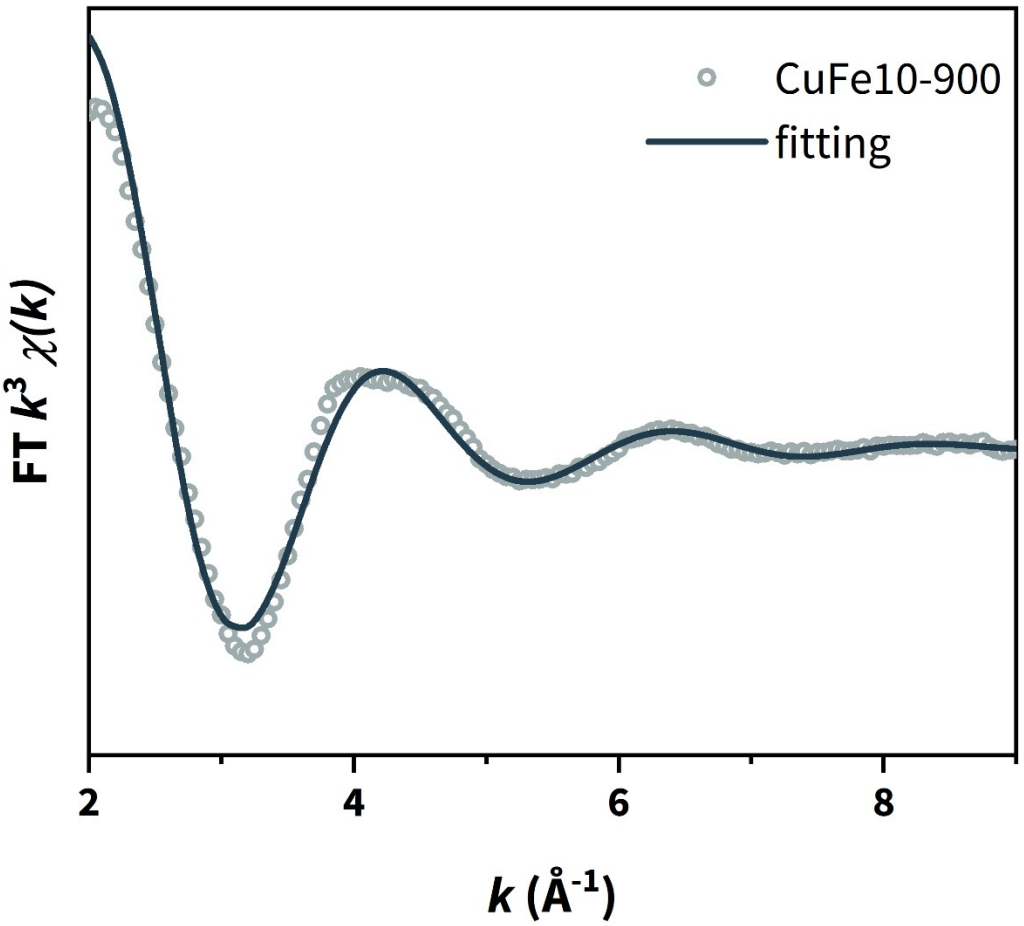

Fig. S12. first-shell Fe-Fe single scattering path fitting of *k* space Fe K-edge EXAFS spectra of CuFe10-900.

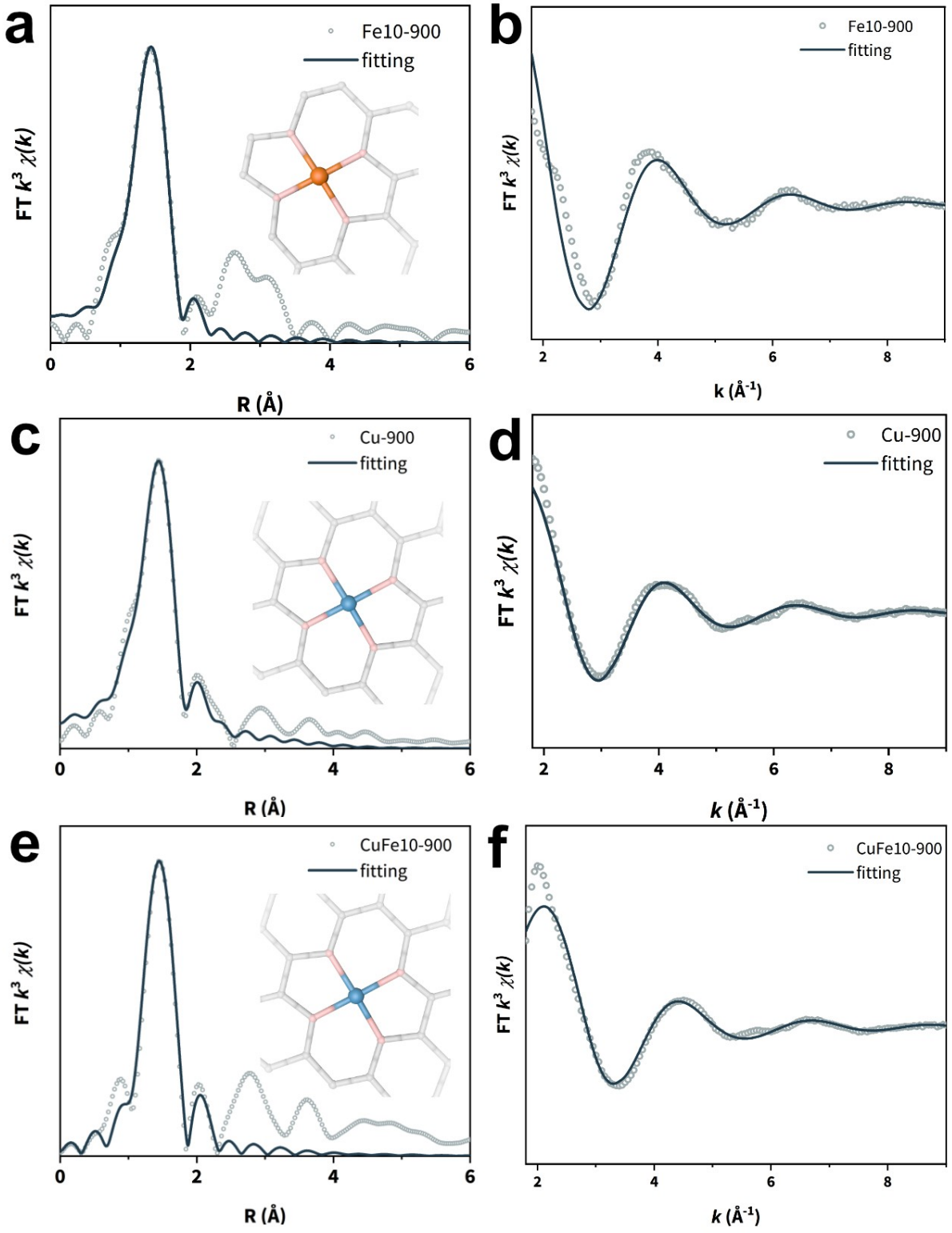

Fig. S13. first-shell Fe-N single scattering path fitting of a) *R* space and b) *k* space of Fe K-edge EXAFS spectra of Fe10-900; first-shell Cu-N single scattering path fitting of c) *R* space and d) *k* space of Cu K-edge EXAFS spectra of Cu-900; first-shell Cu-N single scattering path fitting of e) *R* space and f) *k* space of Cu K-edge EXAFS spectra of CuFe10-900.

sample	Scattering pair	CN	R (Å)	$\sigma^2(10^{-3}Å^2)$	ΔE_0 (eV)	R factor
CuFe10-900	Fe-N	4.3	2.01	9.0	2.5	0.0080
Fe10-900	Fe-N	4.6	1.98	9.5	-7.0	0.013
Fe foil	Fe-Fe1	8	2.46	4.2	4.0	0.0033
	Fe-Fe2	6	2.84			

Table S2. Structural parameters extracted from the Fe K-edge EXAFS fitting. ($S_0^2 = 0.85$)

sample	Scattering pair	CN	R (Å)	$\sigma^2(10^{-3}Å^2)$	ΔE_0 (eV)	R factor
CuFe10-900	Cu-N	3.1	1.91	6.0	5.2	0.0093
Cu-900	Cu-N	3.5	1.95	6.0	-0.9	0.0079
Cu foil	Cu-Cu	12	2.54	8.6	3.9	0.0034

Table S3. Structural parameters extracted from the Cu K-edge EXAFS fitting. ($S_0^2 = 0.85$)

S_0^2 is the amplitude reduction factor, CN is coordination number, R is interatomic distance the bond length between central atoms and surrounding coordination atoms), σ^2 is Debye-Waller factor (a measure of thermal and static disorder in absorber-scatterer distances), ΔE_0 is edge-energy shift (the difference between the zero kinetic energy value of the sample and that of the theoretical model), R factor is used to value the goodness of the fitting.[3]

Error bounds that characterize the structural parameters obtained by EXAFS spectroscopy were estimated as N ± 20%, R ± 1%, σ^2 ± 20%, ΔE_0 ± 20%.

Fe-SAs (FT range: 2.0-11.0 $Å^{-1}$; fitting range: 0.9-2.3 Å),

Fe foil (FT range: 2.0-11.0 $Å^{-1}$; fitting range: 1.3-3.0 Å),

Cu-SAs (FT range: 2.0-11.0 $Å^{-1}$; fitting range: 1.0-2.3 Å),

Cu foil (FT range: 2.0-11.0 $Å^{-1}$; fitting range: 1.1-3.0 Å).

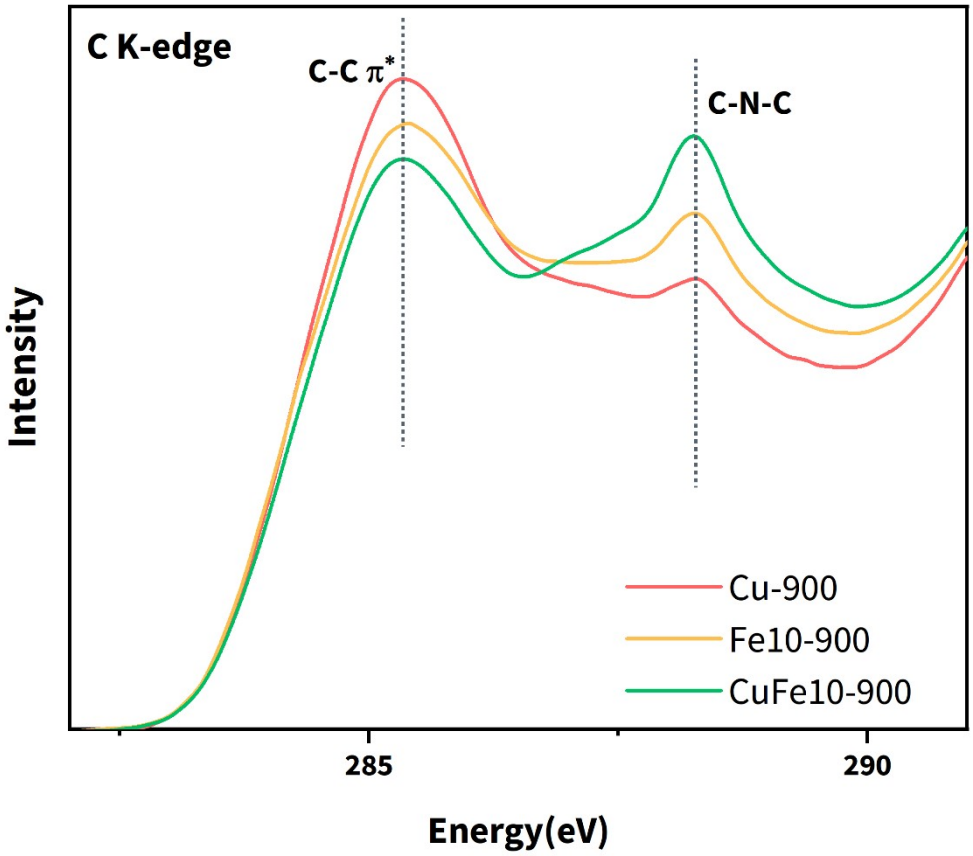

Fig. S14. XANES spectra of C K-edge for three SAC samples.

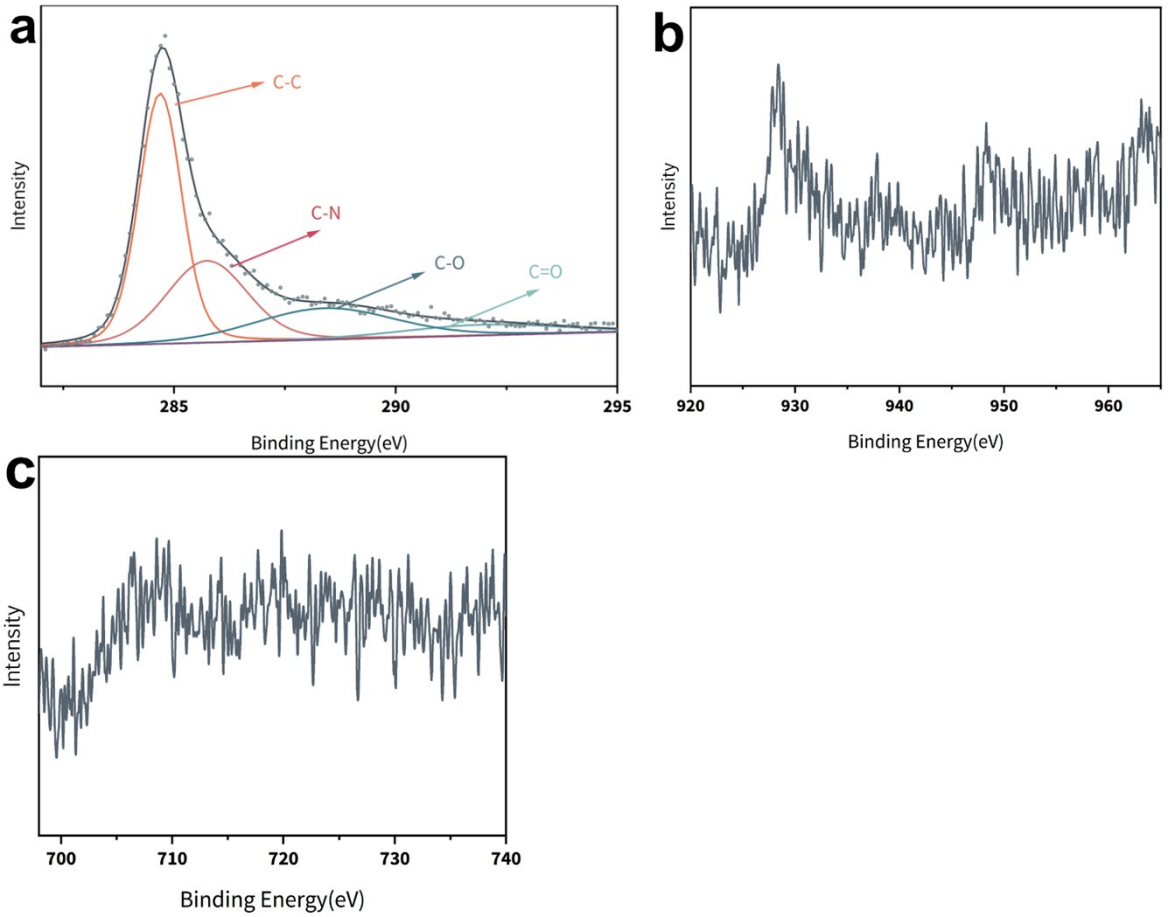

Fig. S15. XPS spectra of (a) deconvoluted C 1s, (b) Cu 2p and (c) Fe 2p for CuFe10-900.

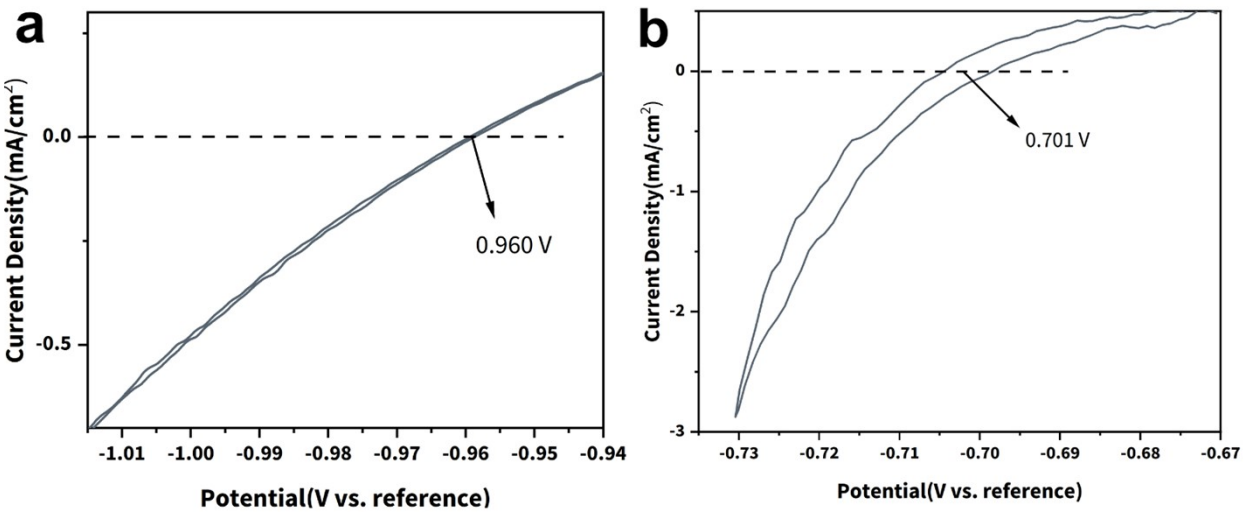

Fig. S16. RHE calibration of reference electrodes: a) AgCl/Ag in 0.1 M KOH and b) Hg_2SO_4/Hg in 0.5 M H_2SO_4.

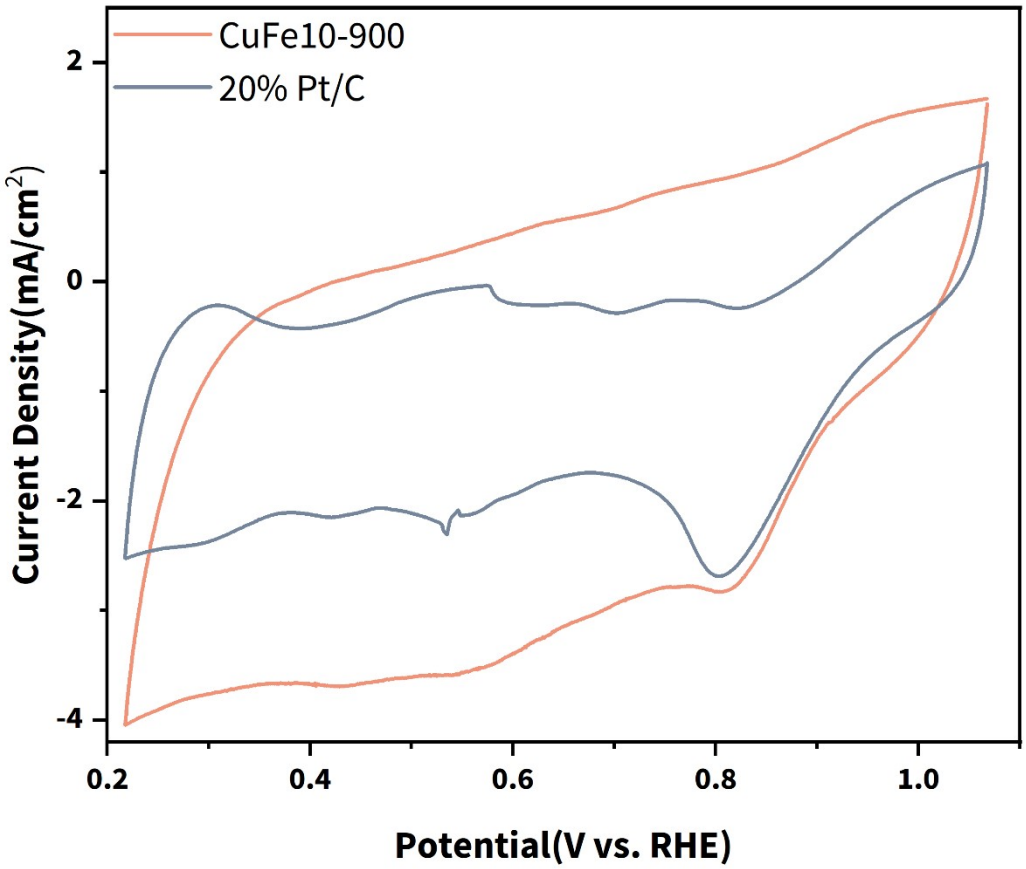

Fig. S17. CV curves in oxygen-saturated 0.1 M KOH.

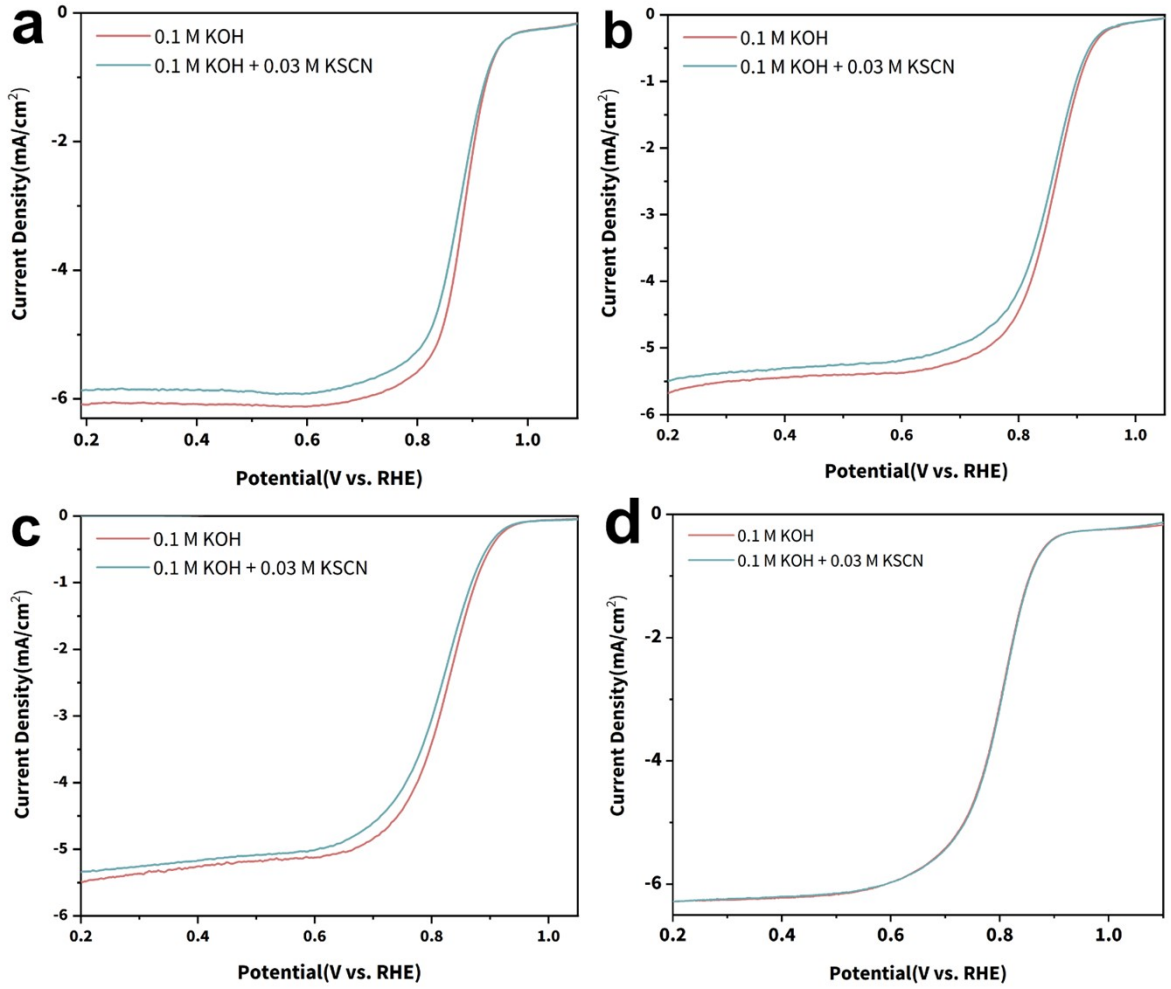

Fig. S18. LSV curves of a) CuFe10-900, b) Fe10-900, c) CuFe20-900 and d) Cu-900 in O_2-saturated KOH with and without KSCN .

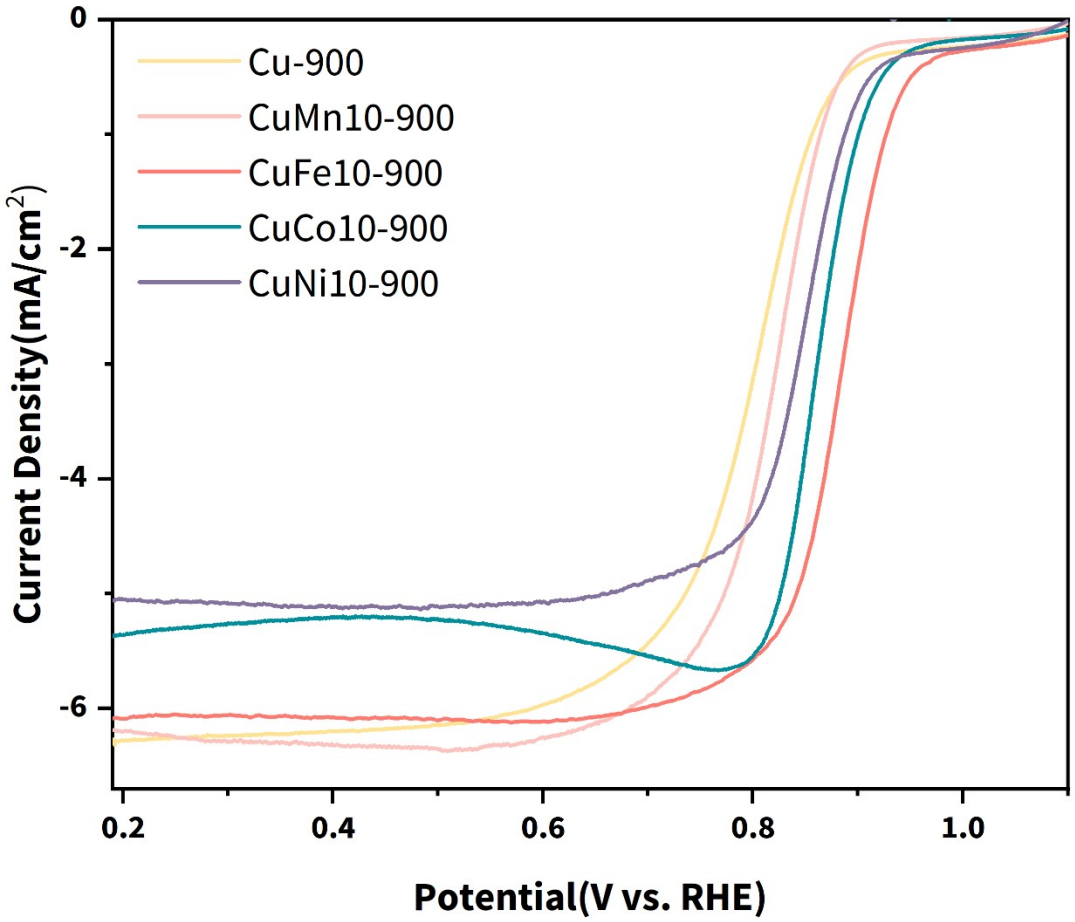

Fig. S19. ORR polarization curves of Cu-900 and CuX-900 (X= Mn, Fe, Co, Ni) in O_2-saturated KOH..

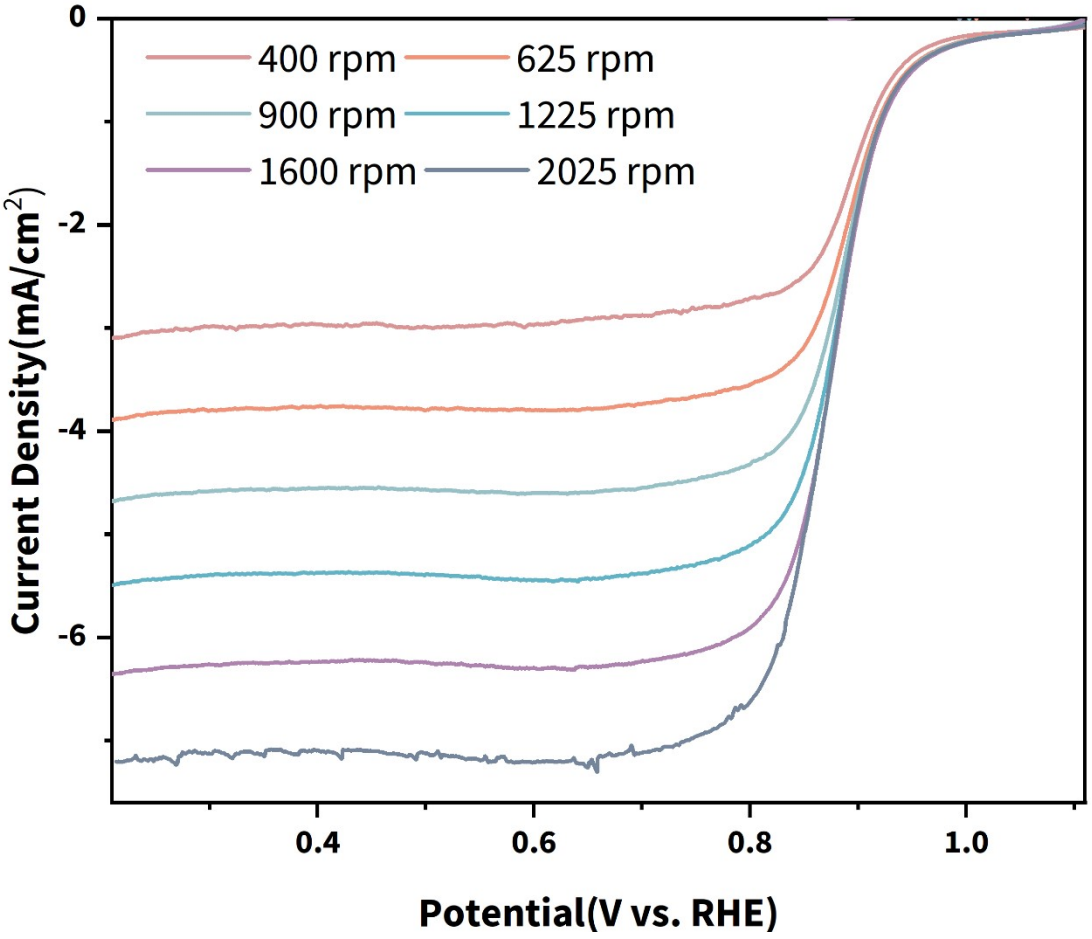

Fig. S20. ORR polarization curves at different rotation rates for CuFe10-900.

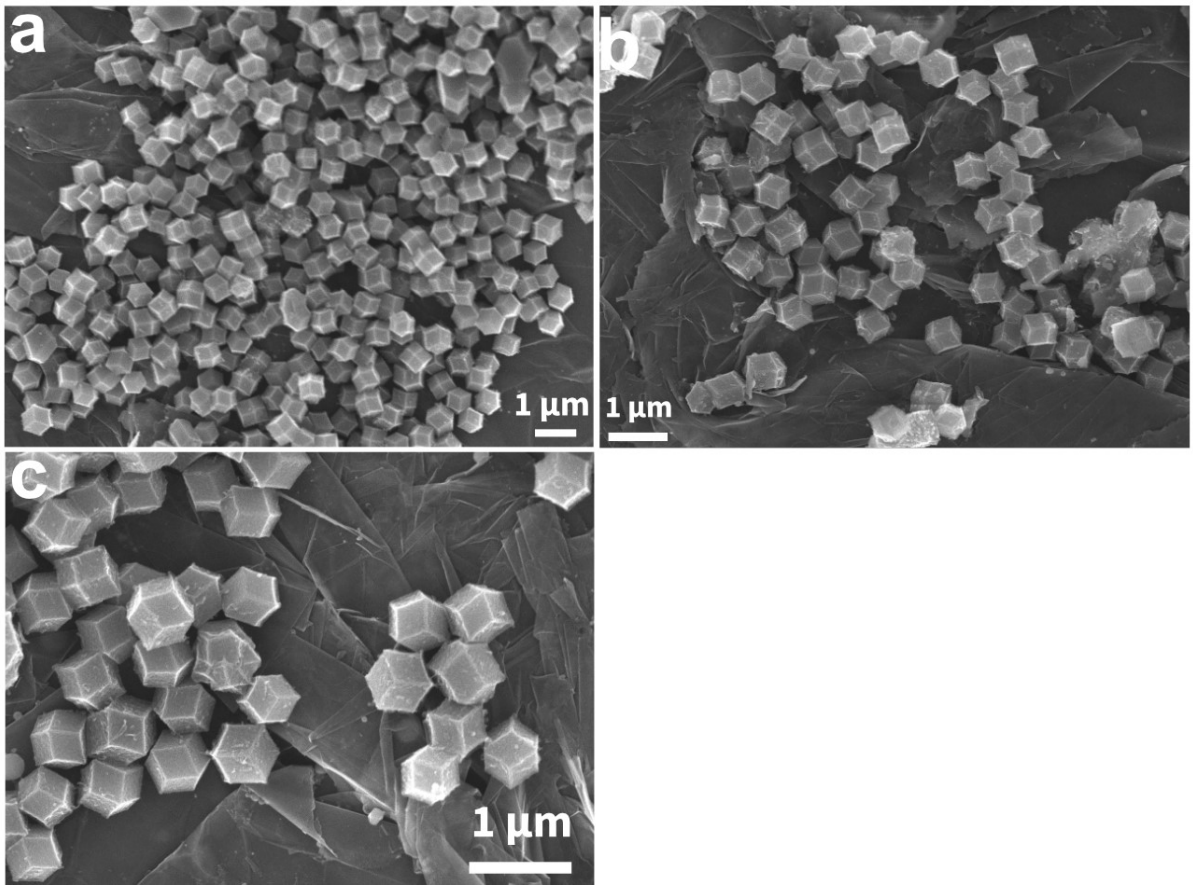

Fig. S21. a-c) SEM images of CuFe10-900 on carbon paper after chronoamperometric test with different magnifications.

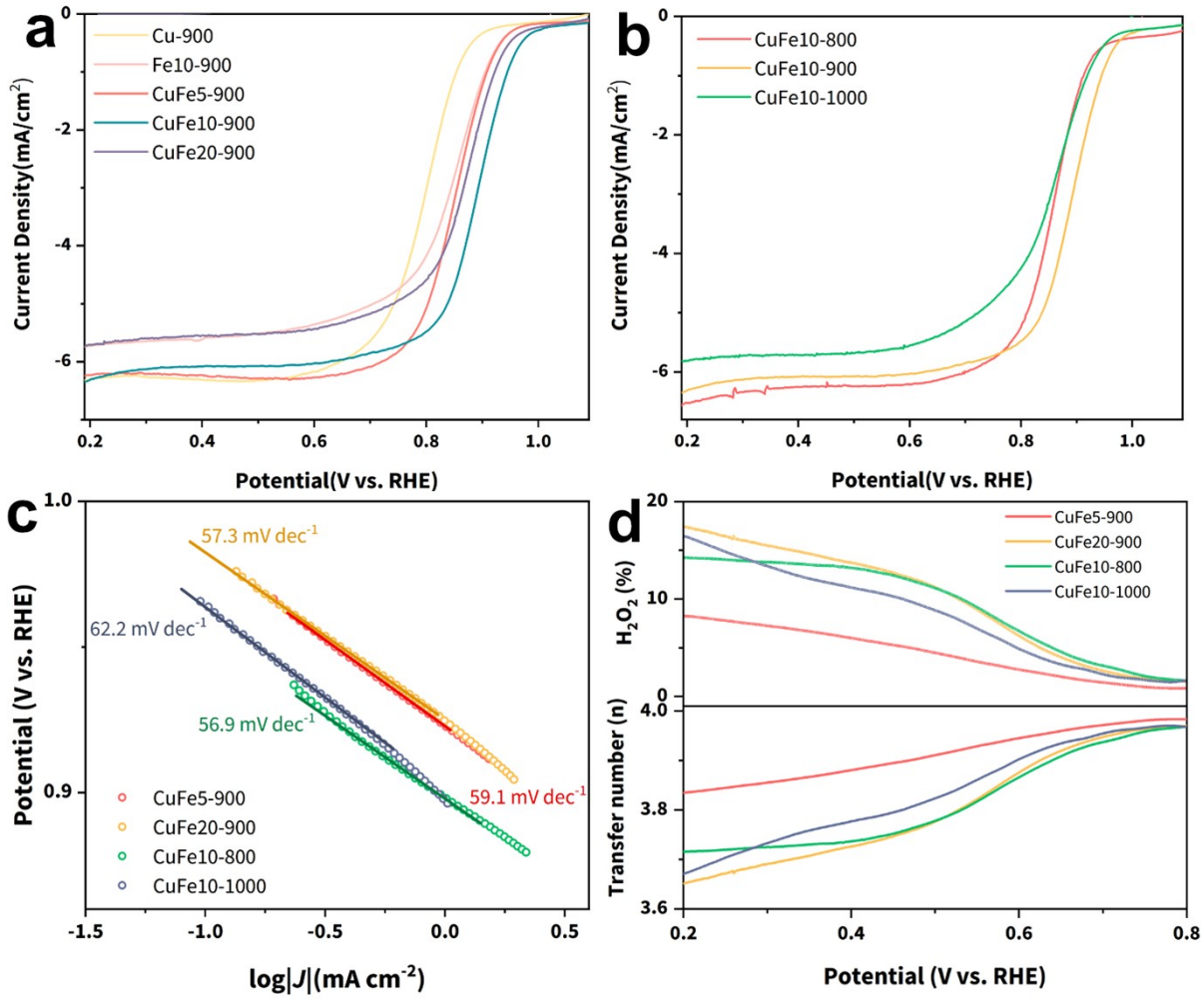

Fig. S22. a) LSV curves of Cu-900, Fe10-900 and CuFex-900 (x=5, 10 and 20), b) LSV curves of CuFe10-800, CuFe10-900 and CuFe10-1000, (c) Tafel plot and (d) H_2O_2 yield and electronic transfer number of CuFe5-900, CuFe20-900, CuFe10-800 and CuFe10-1000.

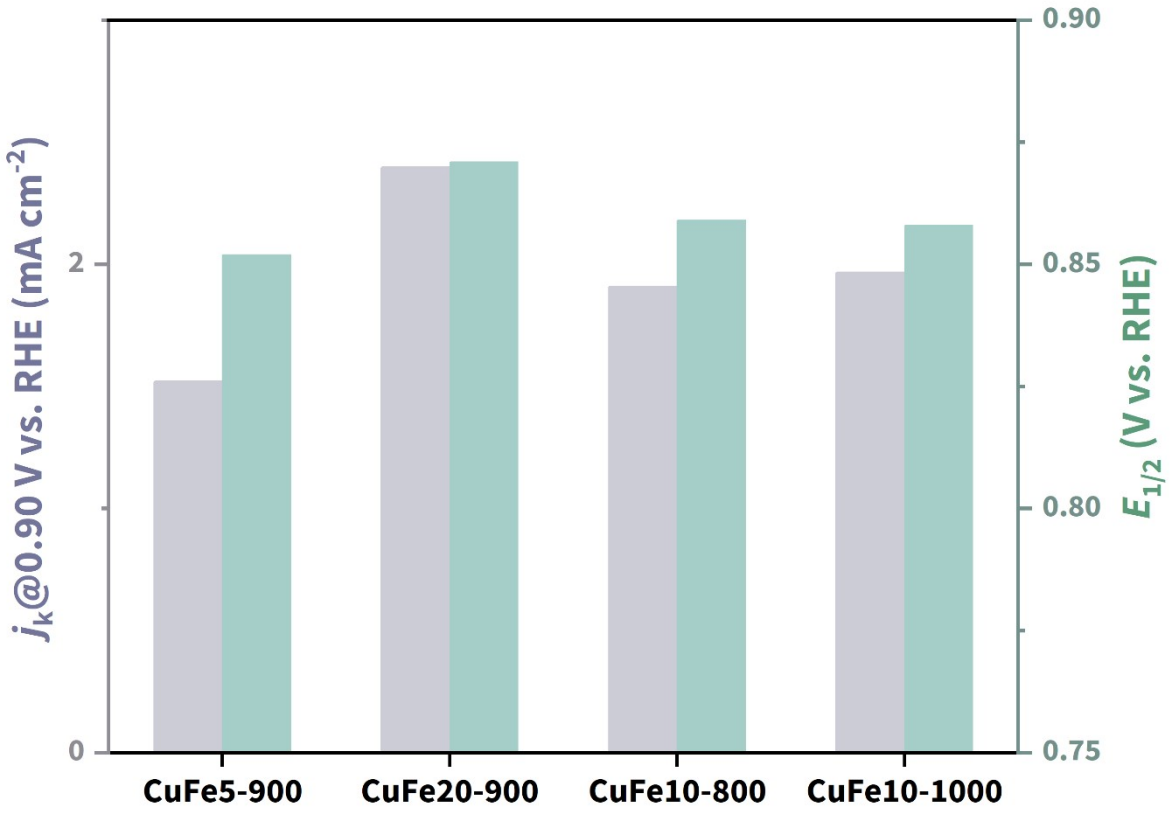

Fig. S23. j_k@0.9 V vs. RHE and $E_{1/2}$ of CuFe5-900, CuFe20-900, CuFe10-800 and CuFe10-1000.

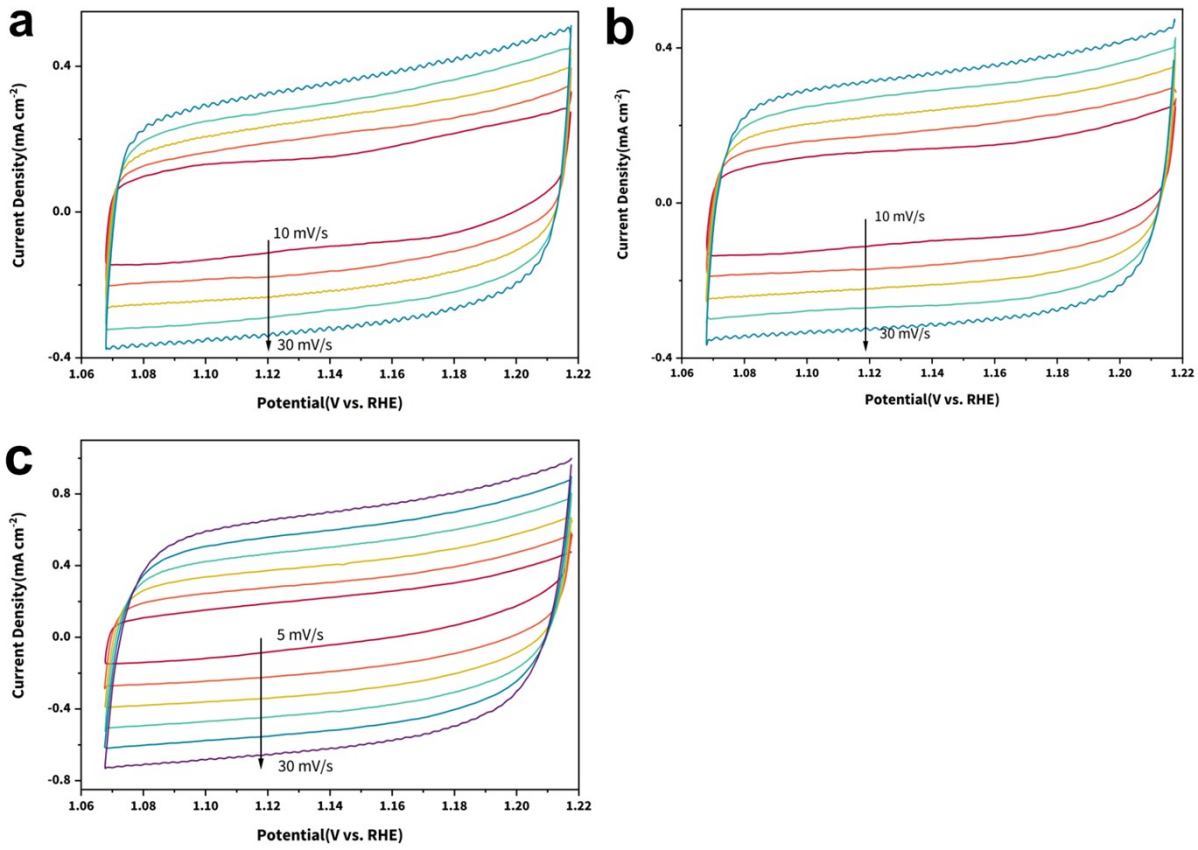

Fig. S24. CV curves with different scanning rates in non-faradaic region: a) Cu-900, b) Fe10-900, c) CuFe10-900.

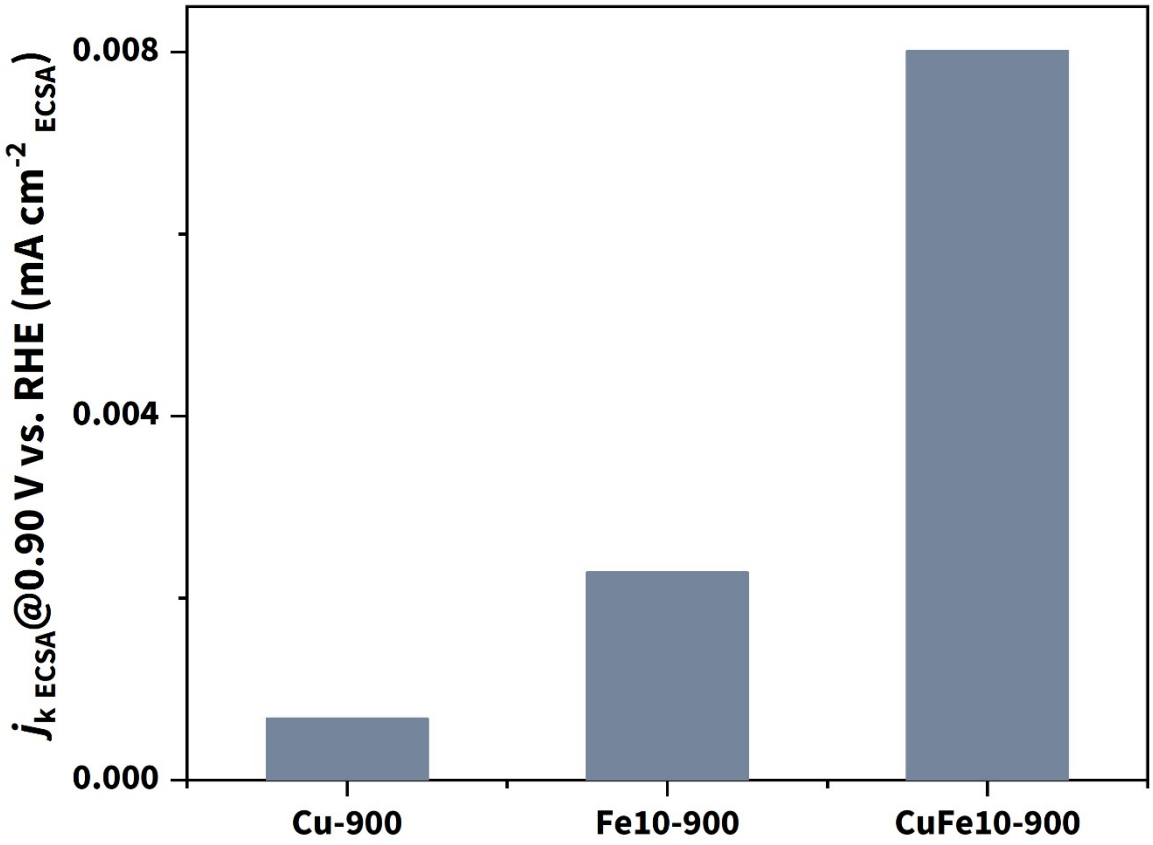

Fig. S25. Comparison of ECSA normalized j_k of three SACs.

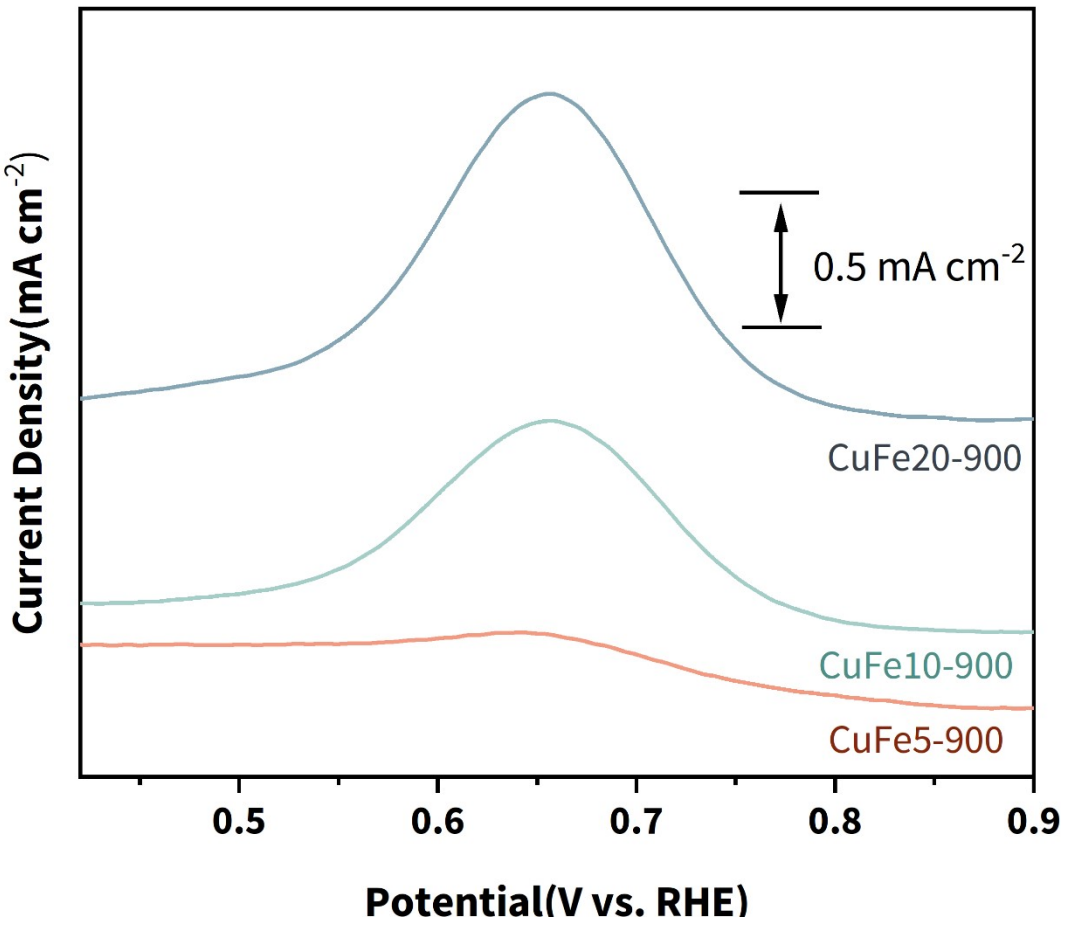

Fig. S26. SWV curves of CuFex-900.

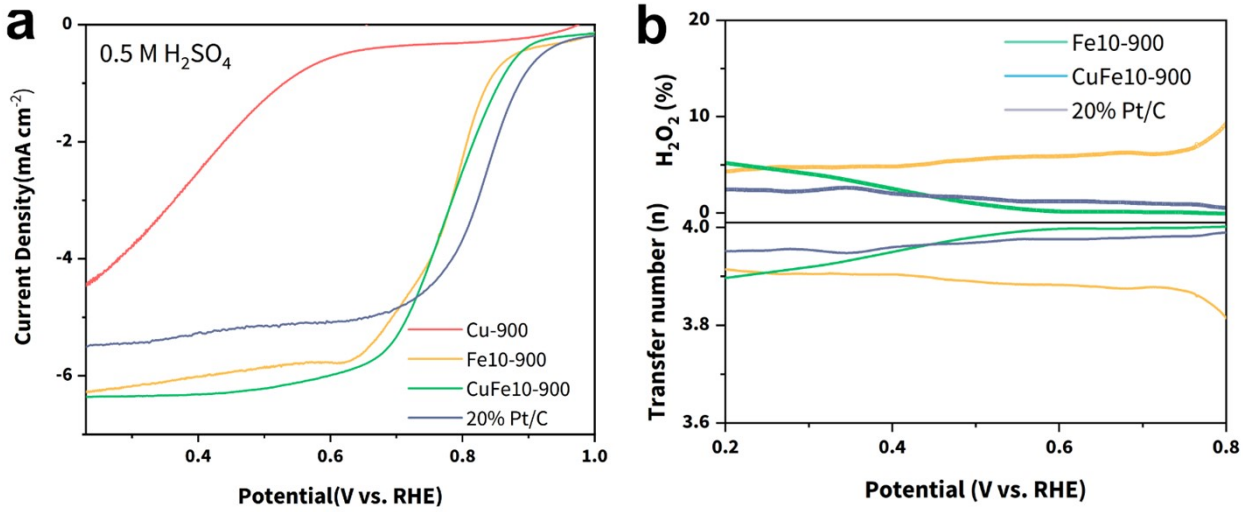

Fig. S27. (a) LSV curves of three SACs and 20% Pt/C, (b) hydrogen peroxide yield and electron transfer number of three samples in 0.5 M H_2SO_4.

SACs	$E_{1/2}$ in alkaline media	$E_{1/2}$ in acidic media	References
CuFe10-900	***0.889***	***0.78***	***This work***
Fe10-900	***0.856***	***0.78***	***This work***
Fe-N/P-C	0.867	0.72	*J. Am. Chem. Soc.* 2020, 142, 2404
SA-Fe-HPC	0.89	0.82	*Angew. Chem. Int. Ed.* 2018, 57, 9038
Fe_{SA}-N-C	0.891	0.776	*Angew. Chem. Int. Ed.* 2018, 57, 8525
Fe/OES	0.85	~0.72	*Angew. Chem. Int. Ed.* 2020, 59, 7384
Fe/Meso-NC-1000	0.885	-	*Adv. Mater.* 2022, 34, 2107291
Fe1-HNC-500-850	0.842		*Adv. Mater*. 2020, 32, 1906905
Fe–N–NDC-1-900	0.89	-	*J. Mater. Chem. A* 2021, 9, 5556
Fe/N-CNRs	0.9	0.73	*Adv. Funct. Mater.* 2021, 31, 2008085
Zn/Fe_2-N-C	0.86	0.81	*J. Mater. Chem. A* 2020, 8, 7145
Fe/N/S-PCNT	0.84	-	*J. Mater. Chem. A* 2019, 7, 1607

Table S4. Brief comparison of Fe-SACs based catalyst for ORR in recent literature.

References

1. Y. Liang, Y. Li, H. Wang, J. Zhou, J. Wang, T. Regier and H. Dai, *Nat. Mater.*, 2011, **10**, 780-786.
2. H. Yang, B. Wang, H. Li, B. Ni, K. Wang, Q. Zhang and X. Wang, *Adv. Energy Mater.*, 2018, **8**, 1801839.
3. Y. Chen, S. Ji, S. Zhao, W. Chen, J. Dong, W. C. Cheong, R. Shen, X. Wen, L. Zheng, A. I. Rykov, S. Cai, H. Tang, Z. Zhuang, C. Chen, Q. Peng, D. Wang and Y. Li, *Nat. Commun.*, 2018, **9**, 5422.